Composites Science and Technology 72 (2012) 886–893

Contents lists available at SciVerse ScienceDirect

Composites Science and Technology

journal homepage: www.elsevier.com/locate/compscitech

Interfacial reactions and wetting in Al–Mg/oxide ceramic interpenetrating composites made by a pressureless infiltration technique

Jing Liu *, Jon Binner, Rebecca Higginson, Zhaoxia Zhou

Department of Materials, Loughborough University, Loughborough LE11 3TU, UK

ARTICLE INFO

Article history:
Received 5 November 2011
Received in revised form 15 February 2012
Accepted 18 February 2012
Available online 25 February 2012

Keywords:
B. Interface
D. Electron energy loss spectroscopy (EELS)
D. Electron microprobe analysis
E. Chemical vapour deposition (CVD)

ABSTRACT

The present paper considers the microstructures of Al–Mg/oxide ceramic interpenetrating composites made by a pressureless infiltration technique. The composites were produced using an Al–10 wt.% Mg alloy with two oxide ceramic foams, spinel ($MgAl_2O_4$) and mullite ($Al_6Si_2O_{13}$), at 915 °C in a flowing N_2 atmosphere. Full infiltration of the aluminium alloy into the ceramic preform has been achieved with good bonding between the metal and ceramic phases. The composites were characterised by a range of techniques and compared with those for alumina from the literature. It has been found that the metal–ceramic interface of the composite consisted of an oxide layer near the ceramic phase and a nitride layer from Mg_3N_2 to AlN near the metal phase. The improvement of Al wetting and adhesion on the oxide ceramics by the addition of Mg and in the presence of N_2 was studied by a sessile drop technique to clarify which compound that formed at the interface contributed to the spontaneous infiltration.

1. Introduction

The development of metal–ceramic interpenetrating composites (IPCs), in which both the metal and ceramic phases are interconnected in three dimensions throughout the whole structure, has resulted in a group of materials with superior properties to traditional MMCs [1]. Among various infiltration techniques for the fabrication of IPCs (e.g. squeeze casting and vacuum infiltration), the pressureless infiltration of molten metals into ceramic preforms is potentially superior as it does not require high pressures, hence there is less risk of preform damage or limitation of preform shape [2].

A high degree of wetting between the molten metal and the solid ceramic phases is crucial for the pressureless infiltration process as positive capillary pressure resulting from good wetting is the governing principle [1]. In addition, good wetting can also yield strong bonding between the metal and ceramic phases, promising superior mechanical properties in the final composite. However, it is known that aluminium often displays poor wettability with oxide ceramic materials. Methods for improving wetting for pressureless infiltration include the use of high temperatures and a controlled atmosphere, alloying the metal and coating the ceramic [3,4].

It has been found that the spontaneous infiltration of Al into Al_2O_3 preforms can occur in the presence of both Mg and N_2 [2,4–6], and there are several explanations of the possible infiltration mechanisms. Srinivasa Rao and Jayaram [2] stated that the initiation of the infiltration was caused by the reaction of Mg with the surface Al_2O_3 to form $MgAl_2O_4$, MgO and Al. These reaction products erode the passivating Al_2O_3 layer and brought about the contact between the molten metal and the ceramic. Then the continuation of the infiltration was due to the Mg gathering O_2 and hence keeping the molten metal front free of passivating Al_2O_3. They observed the formation of $MgAl_2O_4$ and AlN around the alumina particles, but did not investigate their effects on the infiltration process. Saravanan et al. [7] reported that the surface tension of Al in N_2 was greatly reduced compared to the values obtained in Ar at temperatures higher than 850 °C, but this effect was still too weak to induce spontaneous infiltration unless enhanced by alloying additions. Sercombe and Schaffer [8] concluded that during the infiltration of Al alloys into partially nitrided aluminium powder preforms, the formation of AlN improved the wettability and facilitated spontaneous infiltration. Mg was thought to be beneficial in scavenging the oxygen and consequently creating a microclimate with extremely low oxygen partial pressure that facilitated the formation of the AlN. Chang et al. [9] indicated that spontaneous infiltration was dependent on a two-step reaction: Mg and N_2 to form Mg_3N_2 and then the Mg_3N_2 and Al to form AlN on the surface of the Al_2O_3. They suggested that the AlN improved the wetting and hence accelerated the penetration of the molten Al into the ceramic preform. Besides acting as a catalyst for the formation of AlN, they also suggested other roles for the Mg in the infiltration, for example, the presence of Mg at the interface and the formation of $MgAl_2O_4$ on the surface of the Al_2O_3 might be beneficial in terms of reducing interfacial energy and improving wettability.

* Corresponding author. Tel.: +44 (0) 7411 698539; fax: +44 (0) 1509 223949.
E-mail addresses: j.liu2@lboro.ac.uk, xuepaoliujing@msn.com (J. Liu).

0266-3538
doi:10.1016/j.compscitech.2012.02.018

The objectives of this research were to apply the pressureless infiltration technique to the fabrication of IPCs made from Al–Mg alloy and other oxide ceramic materials beside Al_2O_3, e.g. $MgAl_2O_4$ and $Al_6Si_2O_{13}$, and compare their infiltration mechanism(s). The fine scale microstructures at the metal–ceramic interface have been observed and analysed to provide valuable information. In addition, sessile drop tests have been used for each compound that was found at the interfacial area, to see which one(s) was wetted by the molten aluminium and hence induced the infiltration.

2. Experimental

Al–Mg alloys were produced from commercially pure Al and a Mg–Al master alloy, AZ81, by an approach described in [6]. The Al–Mg alloys contained 10 wt.% Mg, as it is reported that with this composition the infiltration rate reached the maximum value [6]. Spinel ($MgAl_2O_4$) and mullite ($Al_6Si_2O_{13}$) foams were produced using a gel-casting technique by Dysons Thermal Technology (Dysons TT) Limited, UK [10]. The density of the foams varied from 15% to 40% and the average cell size was controlled in the range of 100–500 μm. In the pressureless infiltration process, the heating-up stage of the metal and ceramic foam assemblies was performed in pure argon to prevent excessive nitridation of the metal until the desired temperature was reached, and then the furnace atmosphere was changed to pure N_2 to initiate the spontaneous infiltration. When the infiltration was complete, as observed through a quartz glass window at one end of the tube furnace, the composite was cooled in pure argon [9].

A LEO VP 1530 Field Emission Gun Scanning Electron Microscope (FEGSEM) was used to examine the microstructures of the IPCs. The IPC samples were ground and metallographically polished using 1 μm diamond paste before being examined in the FEGSEM. Thin foil Transmission Electron Microscopy (TEM) samples were taken from across the metal–ceramic interfaces using a FEI Nova 600 Nanolab Dual Beam focused ion beam (DBFIB). TEM samples were examined using a JEOL JEM 2000FX TEM equipped with Oxford Instrument Inca EDX spectroscopy, an FEI TecnaiF20 field emission gun (FEG)TEM/Scanning Transmission Electron Microscope (STEM) and a JEOL 2100 FEGTEM. The FEI Tecnai F20 FEGTEM field emission gun TEM/STEM was fitted with a high angle annular dark field (HAADF) detector, Oxford Instruments INCA EDX system/80 mm^2 X-Max silicon drift detector, which provided X-ray elemental maps for Al, Mg, Si, N and O due to the high count rates. The JEOL 2100F was equipped with a Gatan image filter (GIF) Tridiem for electron energy loss spectroscopy (EELS), which provided further analysis of the N and O at the interface with greater spatial resolution and accuracy.

Sessile drop experiments were carried out using sintered ceramic substrates made from the ceramic powders that had been used to fabricate the ceramic foams. The materials examined were pure Al (99.99%), Al–10 wt.% Mg alloy, Al_2O_3 (purity 99.8%), $MgAl_2O_4$ (78wt.% alumina), $Al_6Si_2O_{13}$ (calcined from kyanite (Al_2SiO_5), so that the powder consisted of a major mullite phase and a minor amount of alumina and free silica), and Mg_3N_2 coated on each kind of ceramic substrates using a chemical vapour deposition (CVD) method. The metal specimens, each of about 300 mg, were ultrasonically cleaned in acetone before the wetting tests. The ceramic substrates were ground and polished with diamond suspension to a finish of 1 μm. The wetting tests were performed in an Ar atmosphere and a N_2 atmosphere at 915 °C, which is considered to be the optimum infiltration temperature for the Al/Al_2O_3 system [6]. The contact angles were measured after the metal–ceramic assembly had been heated at 915 °C for 30 min, as it has been observed that all alumina, spinel and mullite foams with 1 cm thickness could be completely infiltrated by the molten Al–Mg alloy in this time. Due to the gas convection in the furnace chamber, the drop shape definition was not entirely satisfactory, resulting in a relatively poor accuracy of contact angle measurements (±3°).

3. Results and discussion

3.1. Microstructures of the interpenetrating composites

An SEM electron-micrograph of a 20% dense spinel foam is shown in Fig. 1a. It can be seen that the gel-cast foam had open and near-spherical cells that are connected by circular windows, providing paths for molten metal to infiltrate in and throughout the whole structure. The mullite foams used in this study had

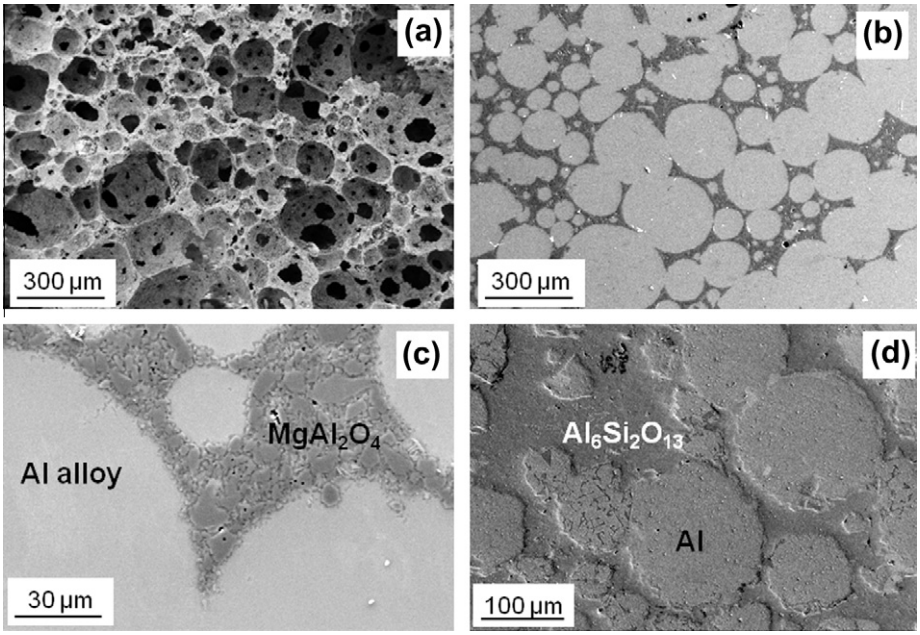

Fig. 1. SEM micrographs of (a) 20% dense spinel foam, IPCs made from Al–10Mg alloy and (b and c) 20% dense spinel foam, and (d) 40% dense mullite foam.

fundamentally the same structure as the spinel foams. SEM micrographs of the infiltrated spinel composites are shown in Fig. 1b and c. The darker regions correspond to the ceramic phase and the bright phase is Al–Mg alloy. It can be seen that the foam was completely infiltrated, except a few closed pores in the ceramic struts. No bulk secondary phases were observed in the composites. From Fig. 1c, no pores or voids are visible in the metal or the interface, indicating good bonding between the metal and the ceramic phases. The mullite-based IPC has a similar structure to the spinel IPC at the "macro"-scale, Fig. 1d. However, a small amount of a second phase is distributed in the metal phase and along the metal–ceramic interface. The major composition of this second phase has been identified as Mg_2Si [11].

A STEM micrograph with EDS maps for the thin foil sample from metal–ceramic interface of the spinel-based composite are shown in Fig. 2. Generally the ceramic phase and the aluminium phase can be distinguished in Fig. 2d, in which the ceramic phase reveals the highest oxygen concentration at the left side and the metal phase reveals the lowest oxygen concentration at the right side. The Mg was observed everywhere, Fig. 2c, as both the aluminium alloy and the spinel phases contained it. A few regions show the highest Mg concentration with the lowest Al concentration, e.g. points A and B in Fig. 2b and c. They were identified by their TEM diffraction patterns as MgO, Fig. 3. This was possibly formed from the reaction of Mg vapour with residual O_2 that had been trapped in the ceramic foam. In addition, some nitride crystals were formed in the Al phase, e.g. points C and D marked in Fig. 2e, and they were identified by their diffraction patterns as AlN [11]. Furthermore, a continuous nitride layer was observed along the metal–ceramic interface in Fig. 2e. Due to the small thickness (<100 nm) of the layer, it could not be identified by TEM diffraction pattern.

A STEM micrograph, with EDS maps, for the metal–ceramic interface of the mullite composite is shown in Fig. 4. From the EDS maps, it can be seen that the region, marked as A at the right side of Fig. 4b, was Al. Near to the Al is a region rich in Si, Fig. 4c, partially associated with Mg rich regions, e.g. points B, C and D labelled in Fig. 4c and d, and the rest with O rich regions, e.g. points E and F in Fig. 4c and e; they were identified as Mg_2Si and SiO_2, respectively. In the oxide ceramic phase that is on the left hand side of the silicide region, both mullite and alumina particles were observed, e.g. points G and H respectively in Fig. 4. Some nanocrystals were observed around the mullite particles, e.g. point I, Fig. 4, and they were identified as $MgAl_2O_4$ by the TEM diffraction pattern, Fig. 5. Between the silicide region and the oxide region, a very thin layer of nitride was observed, Fig. 4f.

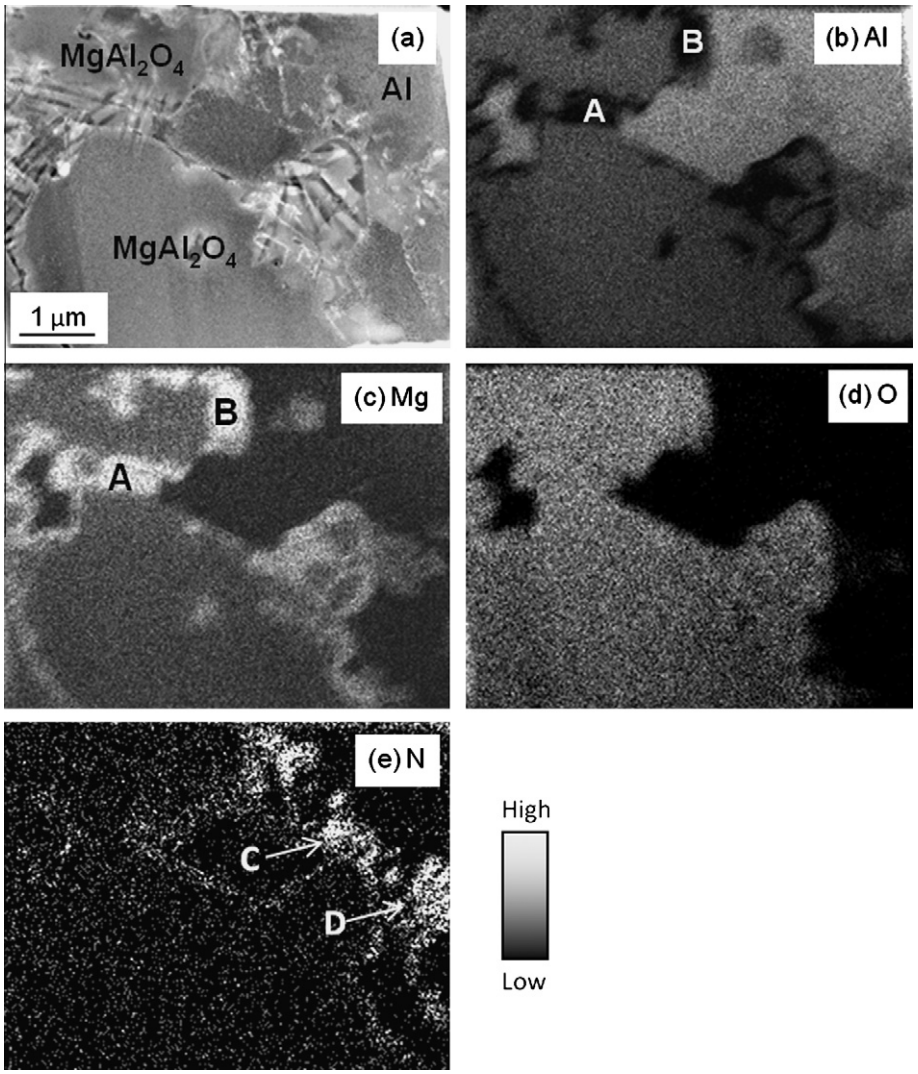

Fig. 2. (a) STEM micrograph of a thin foil lifted out from the metal–ceramic interface in a spinel-based IPC with EDS maps for (b) Al, (c) Mg, (d) O, and (e) N.

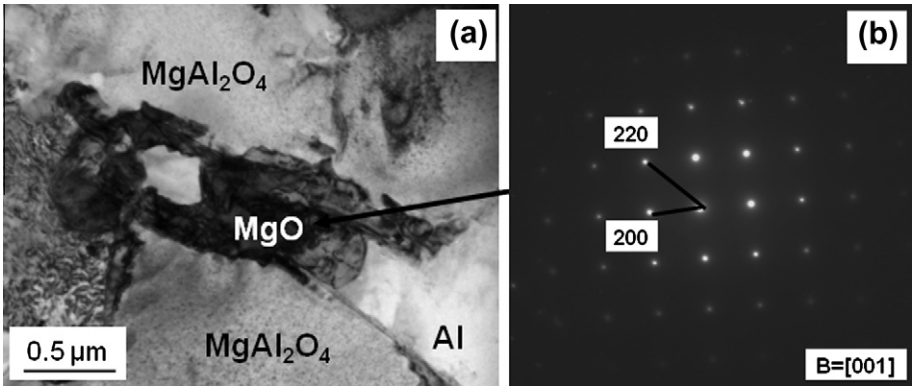

Fig. 3. (a) TEM micrograph and (b) the diffraction pattern of the MgO formed at the metal–ceramic interface in the spinel composite.

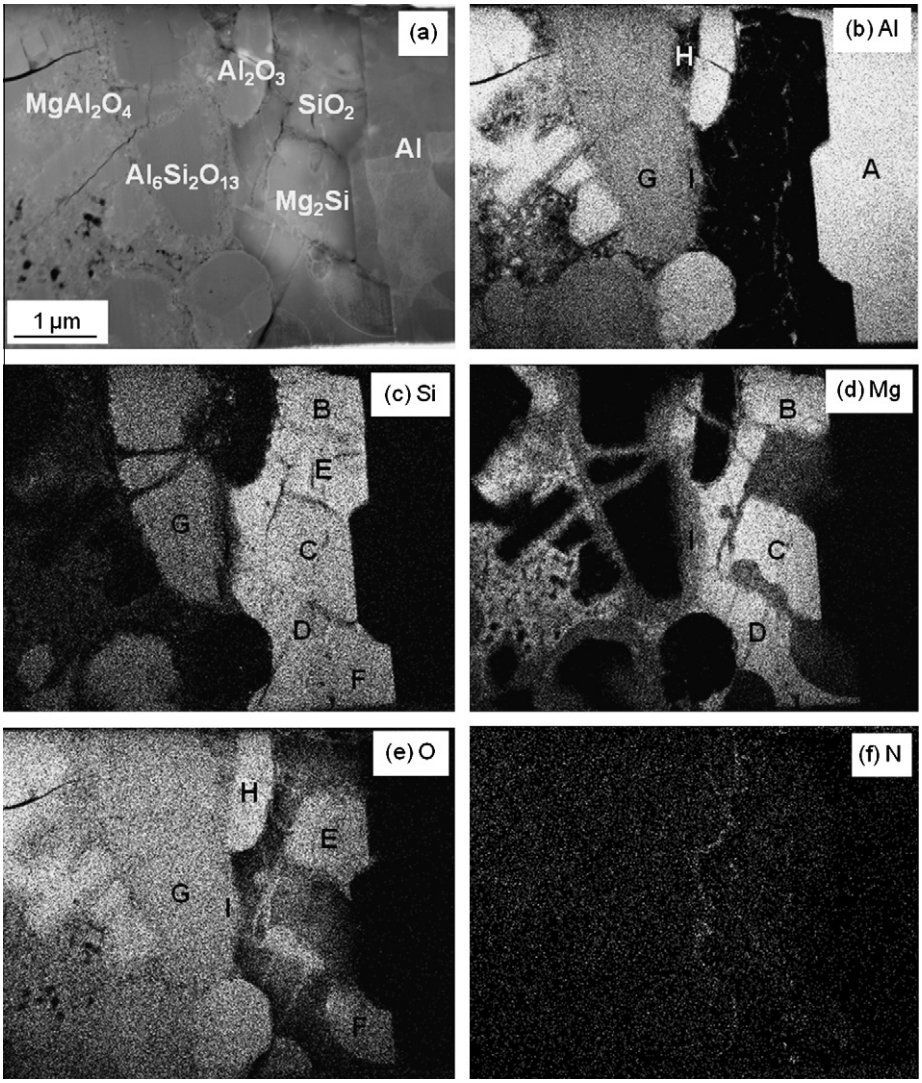

Fig. 4. (a) STEM micrograph of a thin foil sample lifted out from the metal–ceramic interfacial area in an Al(Mg)/$Al_6Si_2O_{13}$ IPC, with EDS maps for (b) Al, (c) Si, (d) Mg, (e) O and (f) N.

As introduced earlier, the mullite powder was calcined from kyanite (Al_2SiO_5) so that the powder consisted of a major mullite phase and a minor amount of alumina and free silica. The silica could react with the Al and Mg, and the possible reactions are:

$$4Al + 3SiO_2 \rightarrow 2Al_2O_3 + 3Si \quad (1)$$

$$2Mg + SiO_2 \rightarrow 2MgO + Si \quad (2)$$

$$2Al + Mg + 2SiO_2 \rightarrow MgAl_2O_4 + 2Si \quad (3)$$

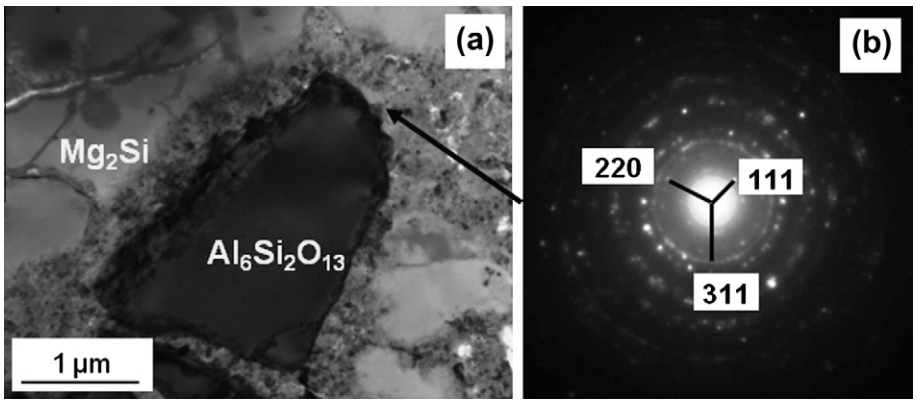

Fig. 5. (a) TEM micrograph and (b) the diffraction pattern of $MgAl_2O_4$ around mullite particles in the mullite-based composite.

In addition, the mullite could react with the molten Al at low oxygen partial pressure and at temperatures above 900 °C [12,13]:

$$3Al_6Si_2O_{13} + 8Al \rightarrow 13Al_2O_3 + 6Si \quad (4)$$

$$\Delta G_{920\,^\circ C} = -1014\ \text{kJ mol}^{-1}$$

Free Si would be released from reactions (1)–(4) and react with the molten metal, forming Mg_2Si after cooling.

It is well known that EDS is not good at identification of light elements, such as N, due to their low fluorescent yield (weak K-lines) and easily absorbed energy by the specimen itself. Since EELS works better for relatively low atomic numbers, to confirm

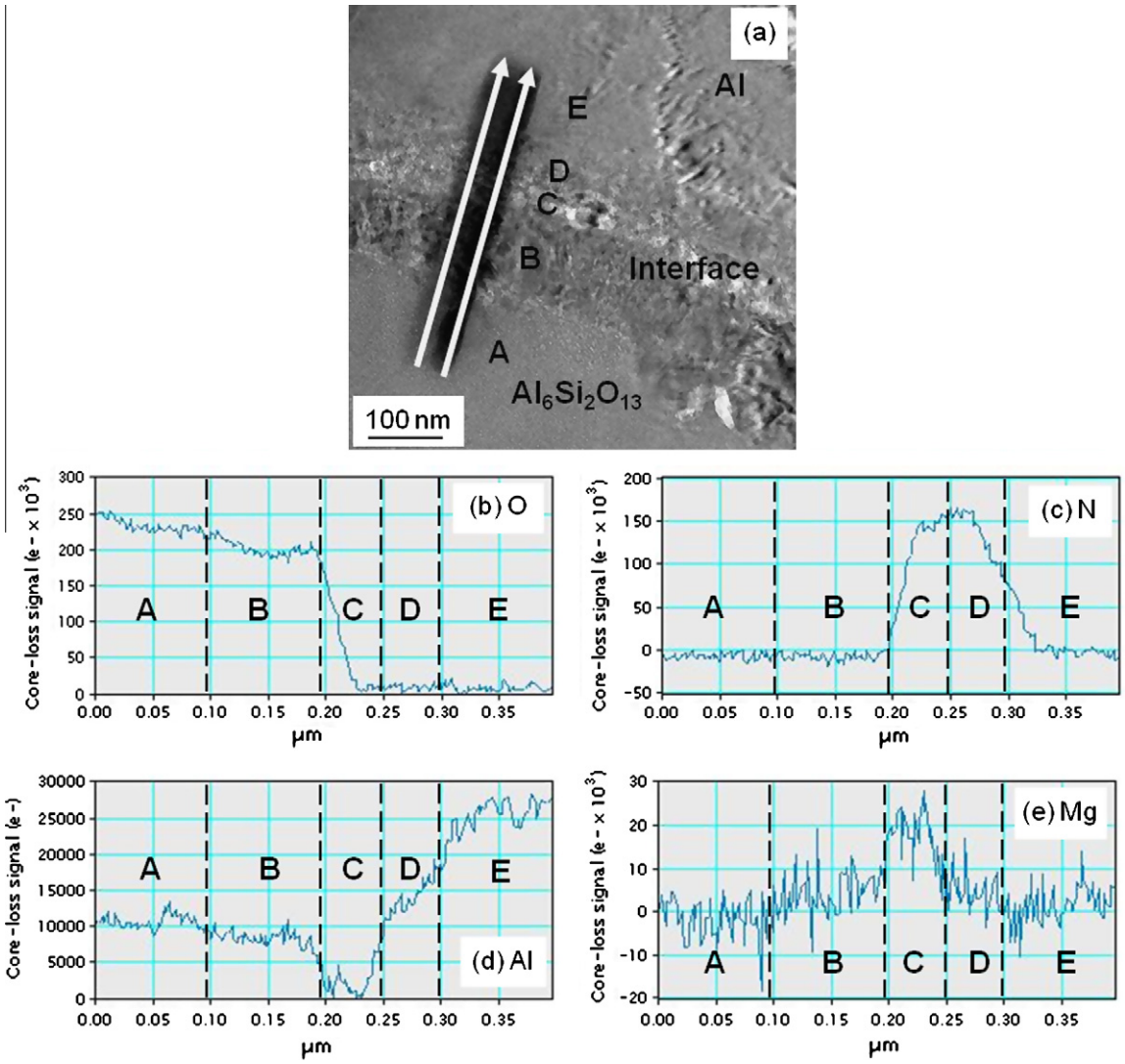

Fig. 6. (a) STEM micrographs of interface of mullite composite, with EELS line scan for (b) O, (c) N, (d) Al and (e) Mg.

further the presence of the continuous nitride layer and identify the detailed composition, the technique was used to analyse a thin foil specimen lifted out from the metal–ceramic interface of the mullite-based composite. A STEM HAADF image of the area is shown in Fig. 6a. The EELS line scans started from the mullite phase and crossed the interface, as indicated. Due to the limited electron energy loss range and the intensity that can be detected at a time, two lines scans were carried out in close proximity, one for O and N K edges and the other for Al and Mg K edges; the results are shown in Fig. 6b–e. The range of 0–0.1 μm from the starting point, i.e. region A marked in Fig. 6, was in the mullite phase, and 0.1–0.2 μm, region B, was in the region of the spinel fine particles that were identified in Fig. 5. In region C, the curve of the O concentration decreased steeply, Fig. 6b, with a significant increase in N concentration, Fig. 6c, suggesting a transition from the spinel layer to a nitride layer. From Fig. 6c, the nitride layer within regions C and D was ~100 nm thick. The Al concentration was very low in region C then increased in region D, Fig. 6d, whilst the Mg showed the opposite distribution, Fig. 6e, being greatest in region C and decreasing in region D. This suggests a transition in the nitride layer that from Mg_3N_2 near the oxide phase to AlN near the metal phase. The coexistence of Mg_3N_2 and AlN formed in two possible ways; one was that the Mg_3N_2 deposited onto the foam surface followed by the deposition of the AlN, and the other was that the Mg vapour reacted with N_2 to form Mg_3N_2, and then the Mg_3N_2 reacted with the molten Al to form AlN [9]:

$$3Mg + N_2 \rightarrow Mg_3N_2 \quad (5)$$

$$\Delta G_{915\,^\circ C} = -213\ \text{kJ mol}^{-1}$$

$$Mg_3N_2 + 2Al \rightarrow 2AlN + 3Mg \quad (6)$$

$$\Delta G_{915\,^\circ C} = -175\ \text{kJ mol}^{-1}$$

From the thermodynamic viewpoint, the formation of both Mg_3N_2 and AlN, i.e. Reactions (5) and (6), are favourable and strongly exothermic, whilst kinetically the formation of Mg_3N_2 is the more favourable reaction when a large amount of Mg vapour is generated than Al due to the higher equilibrium vapour pressure of the Mg than the Al at 900 °C [14]. It is therefore believed that the Mg_3N_2 formed from the reaction of Mg vapour and N_2, deposited and coated the ceramic foam surface. Since the AlN is more stable than Mg_3N_2 at high temperatures, the Al then reacts with the Mg_3N_2 where they were in contact to form the AlN [14].

The EELS maps correlating with Fig. 6a are shown in Fig. 7. Note that the dark line at the left side, indicated by an arrow in Fig. 7a, in the maps was the trace left by the EELS line scan. The nitride layer is clearly shown between the oxide and the Al phases, Fig. 7. Both Mg and Al were present within the nitride region, with opposite distributions, indicating the presence of both Mg_3N_2 and AlN at the metal–ceramic interface, e.g. points A and B marked in Fig. 7, respectively, the former bonding with the metal and the latter close to the oxide. However, the nitride region was not a simple assembly of a Mg_3N_2 layer and a AlN layer with homogeneous thickness; instead, some AlN formed within the Mg_3N_2 region, forming a complex structure. This suggested that the deposition of Mg_3N_2 onto the ceramic surface was porous, so that the Al could have penetrated the Mg_3N_2 layer and react with it to form the AlN.

High-resolution TEM micrographs of the mullite-based composite at the interfaces between the oxide and the nitride, and between the nitride and the metal, are shown in Fig. 8a and b, respectively. In Fig. 8a, the top region was oxide and the bottom was nitride, divided by a dashed line. Good bonding between the oxide and nitride layers was observed and both layers consisted of nanocrystals. In the top right corner of the image, a spinel crystal

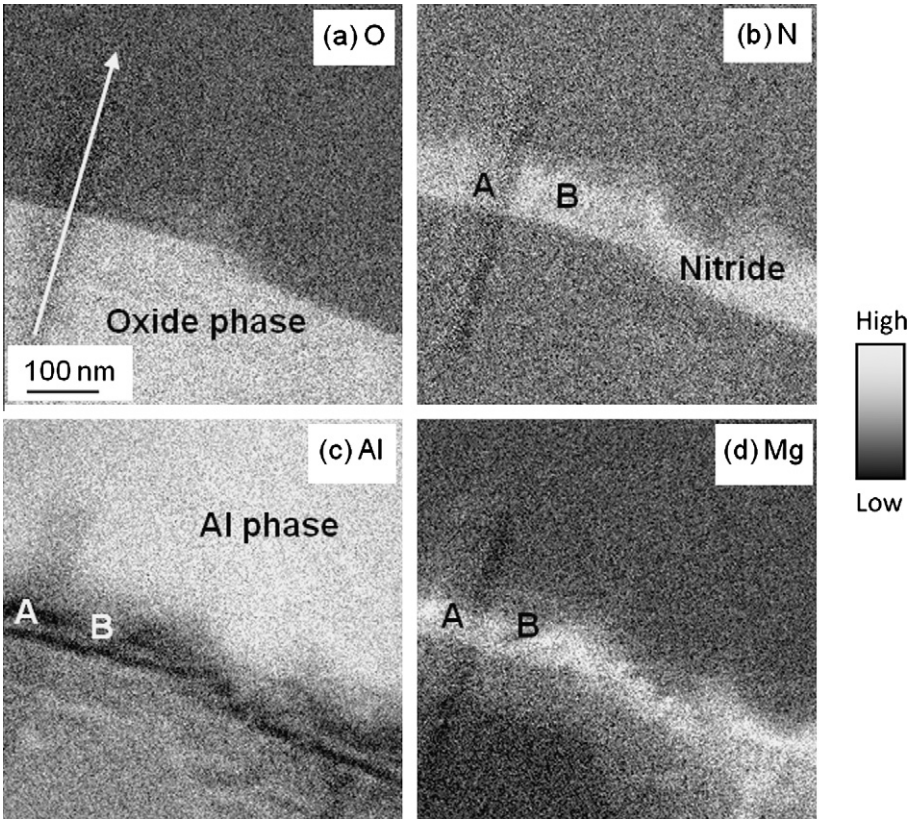

Fig. 7. EELS maps correlating to Fig. 6(a) for (a) O, (b) N, (c) Al and (d) Mg.

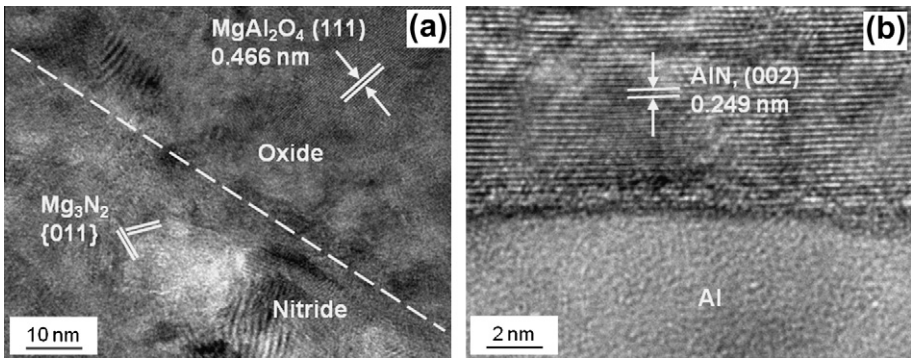

Fig. 8. High resolution images of (a) the bonding between the oxide and the nitride layer, and (b) the bonding between AlN and Al.

Table 1
Contact angles of Al and Al–10Mg on ceramic dense substrates heated at 915 °C for 30 min (±3°).

Materials	Atmosphere	Alumina (°)	Spinel (°)	Mullite (°)
Pure Al	Ar	134	128	135
	N_2	133	124	128
Al–10Mg	Ar	129	121	129
	N_2	116	115	117
Pure Al on Mg_3N_2 coated ceramic plates	Ar	118	102	114
	N_2	27	26	28

can be seen. In the nitride region, the lattice distances and the angle between the lattices, as well as EELS analysis, indicated that one of the crystals was Mg_3N_2. Good bonding between the AlN and Al was also observed, Fig. 8b. Sobczak et al. [15] measured the shear strength of the bonding between AlN and Al and found it was ~60 MPa if the assembly was made at 900 °C and then cooled, whilst an assembly of Al_2O_3 and Al produced at 900 °C yielded a bond strength of ~40 MPa [16].

3.2. Wetting of Al and Al–10Mg on ceramics

According to the results that have been discussed above, four reaction products are generated during the pressureless infiltration process of Al–Mg/$MgAl_2O_4$ and Al/$Al_6Si_2O_{13}$ systems, these are $MgAl_2O_4$, MgO, Mg_3N_2 and AlN. In the previous study at Loughborough University, the same four reaction products were observed in an Al–Mg/Al_2O_3 system fabricated using the same pressureless infiltration technique [9]. Lee et al. [6] found the formation of Mg_3N_2 during the infiltration in an Al/Al_2O_3 system and they stated that the Mg_3N_2 enhanced the wetting between the molten alloy and the ceramic. Some researchers [7,8] argued that it is AlN that improves the wettability and facilitated the spontaneous infiltration. It has also been suggested that the formation of $MgAl_2O_4$ may be beneficial to infiltration in terms of reducing interfacial energy, improving wettability and promoting interfacial bonding [2,6,9]. To clarify which reaction product(s) finally improved the wettability, a series of sessile drop tests were conducted and the results are shown in Table 1. As expected, contacts angles of pure Al on all of the oxide ceramic substrates at 915 °C were larger than

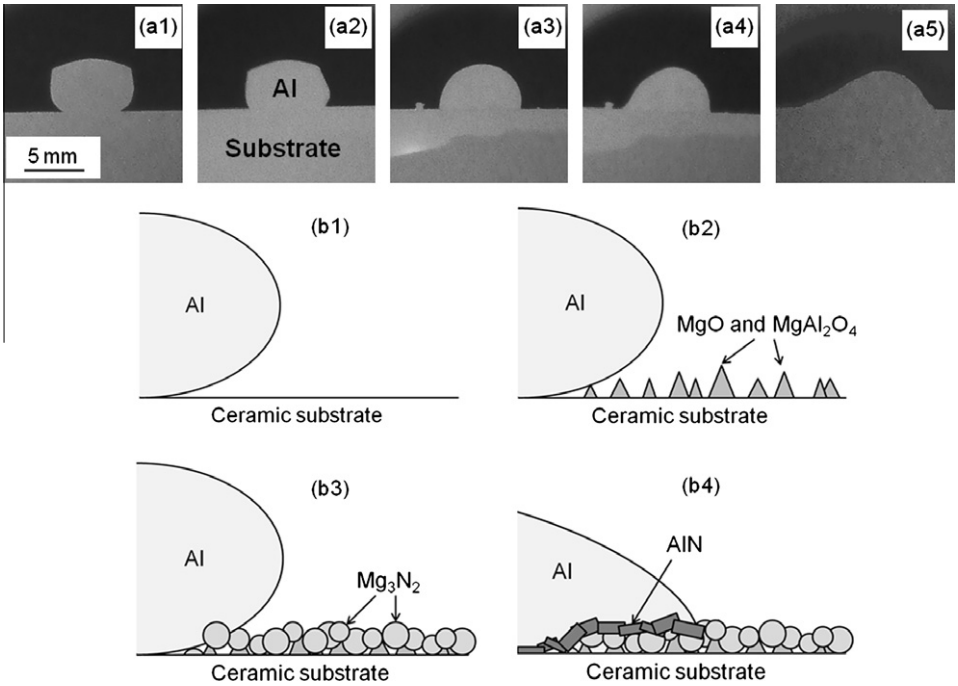

Fig. 9. (a) Wetting behaviour of Al on Mg_3N_2 coated Al_2O_3 substrate at 915 °C in N_2 for (a1) 0 min, (a2) 1 min, (a3) 2 min, (a4) 3 min and (a5) 5 min. (b) Schematics of the reactive wetting process during the pressureless infiltration process: (b1) non-wetting of Al and ceramic phases, (b2) reactions between reactive metals and residual O_2 to form MgO and $MgAl_2O_4$, (b3) reaction between Mg vapour and N_2 to form Mg_3N_2, (b4) reaction between Al and Mg_3N_2 when in contact to form AlN, which was, in turn, wetted by the liquid Al.

90° indicating non-wetting; the presence of the N_2 also did not show a significant influence on the wettability. Although the contact angles were slightly decreased with the addition of Mg into Al, they were greater than 90°. When the ceramic substrates were still coated with Mg_3N_2, observed as greenish-yellow powders, the contact angles of pure Al on the substrates in Ar were larger than 90°, but in N_2 the contact angles dramatically decreased to less than 30°. Fig. 9a1–a5 shows the change of the contact angle of Al on the Mg_3N_2 coated substrate when the N_2 was introduced.

As discussed earlier, the Mg_3N_2 could react with molten Al to form AlN. It has been reported that the contact angle of Al on AlN is ~40° at ~900 °C in vacuum [15]. Therefore, the different contact angles of Al on Mg_3N_2 coated substrates in Ar and N_2, respectively, could be due to the transition of Mg_3N_2 into AlN, which is difficult without N_2, and the fact that Al does not wet the Mg_3N_2. When the N_2 was introduced, the wetting angle gradually decreased from ~120° to ~30°, suggesting a reactive wetting process. It is believed that the Mg_3N_2 reacted with the front of the metal drop and formed AlN enabling the metal to move into the AlN and continue the reaction with the Mg_3N_2. Note that whilst the contact angles of Al–10 Mg on the ceramic substrates in N_2 were larger than 90°, the ceramic foams could be infiltrated by the Al–10 Mg in N_2. This can be explained by the foam being porous, allowing the Mg_3N_2 to deposit everywhere on the foam struts; whilst in the sessile drop test, the Mg_3N_2 could not coat the area where the metal and the substrate were in contact, but only the area around the metal, and, in this situation, the reaction could not occur to form AlN. Based on the results, it appears to be the aluminium nitride rather than the spinel or magnesium nitride that directly improves the wetting. The magnesium nitride aids the spontaneous infiltration via promoting the formation of an AlN coating on the ceramic foam surface. The spinel may assist the infiltration by an additional mechanism where the Mg_3N_2 deposits faster onto the spinel than alumina, resulting in a higher infiltration rate and hence shorter processing time [11]. Fig. 9b1–b4 illustrates the reactive wetting process during the pressureless infiltration process. As mentioned before, all the alumina, spinel and mullite systems revealed the same reaction products at the metal–ceramic interface, so a fundamentally similar reactive wetting process is suggested. The difference between them is the formation of the oxide reaction products, which occurs in the stage shown in Fig. 9b2. The common source of the oxides for the three systems are the reactions between the metal and the residual O_2, whilst the alumina can react with Mg to form spinel, and the silica contained in the mullite foam will react with the metal to form oxide and silicon.

4. Conclusions

Spinel- and mullite-based IPCs have been formed by pressureless infiltration of molten Al–Mg alloy into gel-cast ceramic foams in a sequence of Ar–N_2–Ar atmospheres. Good metal–ceramic interfacial bonding has been observed. TEM and EELS analysis at the interface reveals that MgO, $MgAl_2O_4$, Mg_3N_2 and AlN have all been formed in both the spinel- and mullite-based composites, the latter containing Mg_2Si in the metal phase resulting from reaction of Mg with the released Si from the reactions between the ceramic and the metal. The oxide layer of MgO and $MgAl_2O_4$ was near to the ceramic struts and the continuous, dense nitride layer from Mg_3N_2 to AlN was bonded with the Al alloy. The sessile drop tests suggest a reactive wetting process in the spontaneous infiltration and it was AlN that improved wetting and inducing the infiltration by capillary action. It appears that all three ceramic foams undergo fundamentally the same mechanism during the spontaneous infiltration, in that Mg_3N_2 deposits on the ceramic surface and then reacts with Al to form AlN, which largely reduces the solid/liquid interfacial energy. With the results from this study, it is expected to be able fabricate IPCs from a wide range of aluminium alloys and ceramics.

Acknowledgements

The authors thank Dyson Thermal Technologies, Sheffield, UK, for the supply of the ceramic foams. Thanks are also extended to Dr. Geoff West for the DBFIB operations. We owe a great debt to Dr. Michael W. Fay at Nottingham Nanotechnology and Nanoscience Centre through the UK EPSRC Open Access system for operating the 2100F TEM.

References

[1] Clarke DR. Interpenetrating composites. J Am Ceram Soc 1992;75:739–59.
[2] Srinivasa Rao B, Jayaram V. Pressureless infiltration of Al–Mg based alloys into Al_2O_3 preforms: mechanisms and phenomenology. Acta Mater 2001;49:2373–85.
[3] Sobcazk N, Asthana R, Ksiazek M, Radziwill W, Mikulowski B. The effect of temperature, matrix alloying and substrate coatings on wettability and shear strength of Al/Al_2O_3 couples. Metall Mater Trans A 2004;35:911–23.
[4] Aghajanian MK, Nagelberg AS, Kennedy CR. Method for forming metal matrix composites having variable filler. US Pat. 1991; No. 5020584.
[5] Binner J, Chang H, Higginson R. Processing of ceramic–metal interpenetrating composites. J Eur Ceram Soc 2009;29:837–42.
[6] Lee KB, Kim YS, Kwon H. Fabrication of Al-3 wt pct Mg matrix composites reinforced with Al_2O_3 and SiC particulates by the pressureless infiltration technique. Metall Mater Trans A 1998;29:3087–95.
[7] Saravanan RA, Molina JM, Narciso J, García-Cordovilla C, Louis E. Effect of nitrogen on the surface tension of pure aluminium at high temperatures. Scripta Mater 2001;44:965–70.
[8] Sercombe TB, Schaffer GB. On the role of magnesium and nitrogen in the infiltration of aluminium by aluminium for rapid prototyping applications. Acta Mater 2004;52:3019–25.
[9] Chang H, Higginson RL, Binner JGP. Interface study by dual-beam FIB-TEM in a pressureless infiltrated Al(Mg)–Al_2O_3 interpenetrating composite. J Microsc 2009;233:132–9.
[10] Sepulveda P, Binner JGP. Processing of cellular ceramics by foaming and in situ polymerisation of organic monomers. J Eur Ceram Soc 1999;19:2059–66.
[11] Liu J, Binner J, Higginson R. Processing of oxide ceramic/aluminium alloy interpenetrating composites using pressureless infiltration and its mechanism. Acta Mater, unpublished results.
[12] Soundararajan R, Kuhn G, Atisivan R, Bose S, Bandyopadhyay A. Processing of mullite-aluminium composites. J Am Ceram Soc 2001;84:509–13.
[13] Loehman RE, Ewsuk K, Tomsia AP. Synthesis of Al_2O_3–Al composites by reactive metal penetration. J Am Ceram Soc 1996;79:27–32.
[14] Hou Q, Mutharasan R, Koczak M. Feasibility of aluminium nitride formation in aluminium alloys. Mater Sci Eng A 1995;195:121–9.
[15] Sobczak N, Ksiazek M, Radziwill W, Stobierski L, Mikulowski B. Wetting-bond strength relationship in Al-AlN system. Trans JWRI 2001;30:125–30.
[16] Ksiazek M, Sobczak N, Mikulowski B, Radziwill W, Surowiak I. Wetting and bonding strength in Al/Al_2O_3 system. Mater Sci Eng A 2002;324:162–7.